Green Chemistry

PAPER

"One-for-all" on-demand multifunctional fluorescent amphoteric polymers achieving breakthrough leather eco-manufacturing evolution†

Chao Wei,[a] Xuechuan Wang, [ID] *[a,b] Shuang Liang,[b] Xiaoliang Zou,[b] Long Xie[a] and Xinhua Liu [ID] *[b]

The traditional leather industry holds a significant position within the global manufacturing sector, contributing both economically and socially. Relentless multifunctional material-innovation for sustainable leather-manufacture is the only pathway to completely solve the current environmental concerns including widescale discharge of waste and chemicals. Herein, we address these limitations by developing a scalable and sustainable "one-for-all" strategy based on a synthetic multifunctional fluorescent amphoteric polymer (referred to as AADs) through free radical polymerization and amidation grafting reactions achieving a breakthrough leather eco-manufacturing evolution. The resulting AADs effectively integrate the all-round multifunctionalities of tanning, retanning, fatliquoring, regulable color dyeing, and anti-counterfeiting marking into leather. The interfacial multi-point cross-linking of AADs with natural collagen fibers in leather enhances crust-leather with a shrinkage temperature (T_s) exceeding 77 °C and standard-compliant mechanical properties, scratch resistance, and fluorescence for anti-counterfeiting purposes through the creation of distinctive patterns such as barcodes and QR codes. The formative covalent-bonding between the two significantly enhances dye fixation, resulting in leathers with superior durability against rubbing and washing. This innovative process not only reduces the processing time from 1095–2360 min to 500 min and cuts down leather chemical usage by 47.5–74.8%, but also lowers water consumption by 82.6–90% through streamlining multiple primary procedures into a single process. Furthermore, AADs robustly minimize human health risks by 55–71.6% and decrease greenhouse gas emissions by 38.2–52.4% and environmental impacts by 49.3–58.8%, lowering the carbon and environmental footprint of leather production. The innovation of the "one-for-all" process based on emerging multifunctional materials aligns with global sustainability goals, fundamentally aiding the leather industry in transitioning towards more sustainable practices.

1. Introduction

Currently, to promote the development of a global low-carbon circular economy, the manufacturing industry is increasingly focusing on ecological and sustainable development, a trend that is particularly evident in the traditional leather manufacturing industry. The traditional leather manufacturing sector faces substantial pressure to adapt due to rising environmental awareness and growing consumer demand for sustainable products.[1,2] One of the major environmental challenges faced by this sector is the pollution caused by traditional chrome tanning.[3] Additionally, leather processing involves numerous steps that utilize a variety of chemicals, leading to the inevitable production of plentiful sundry pollutants.[4,5] These environmental issues present technical obstacles that hinder the sustainable development of the leather industry.[6–8] Consequently, the development of chrome-free eco-leather manufacturing technologies and the optimization of tannery processes and related leather chemicals have emerged as the key priorities for the global leather industry.[9]

The resolution of the aforementioned environmental issues relies heavily on the development of streamlined multifunctional ecological leather chemicals.[10–12] In other words, sustainable leather manufacturing can be achieved through the

[a]College of Chemistry and Chemical Engineering, Shaanxi University of Science & Technology, Xi'an 710021, Shaanxi, China. E-mail: wangxc@sust.edu.cn
[b]College of Bioresources Chemical and Materials Engineering, Institute of Biomass & Functional Materials, Shaanxi University of Science & Technology, Xi'an 710021, Shaanxi, China. E-mail: liuxinhua@sust.edu.cn
†Electronic supplementary information (ESI) available. See DOI: https://doi.org/10.1039/d4gc04416a

development of eco-friendly chrome-free tanning and complementary wet-finishing materials, as these processes—including re-tanning, dyeing, and fat-liquoring—utilize a wide range of chemicals, such as tanning agents, fat liquors, and dyestuffs.[13–15] From a fundamental perspective, the development of multi-functional leather chemicals can streamline multiple stages of leather processing, enhancing the ecological viability of chrome-free tanning technologies without compromising on leather quality. Developing biomass-based tanning agents is an effective way to address the pollution caused by chromium tanning. For instance, lignin,[16] hemicellulose,[17] cellulose,[18] starch,[19] chitosan[14] and other raw materials, after chemical modification, can be used to produce chrome-free tanning agents that impart higher shrinkage temperatures as well as improved physical and mechanical properties, sensory attributes, and antimicrobial characteristics to leather. These biomass tanning agents demonstrate satisfactory overall performance. However, the extraction of biomass raw materials is often complex and costly, leading to challenges in ensuring product quality. Furthermore, the fixed structure of biomass materials limits their modification, hindering the practical application of biomass-based tanning agents. Organic chrome-free tanning agents are gradually emerging as viable alternatives to traditional chrome tanning agents due to their abundant monomer sources, customizable structures, cost-effectiveness, and versatile performance characteristics.[19] Significant progress has been made in the development of these agents, including Granofin F-90 organic tanning agent from Clariant Ltd,[20] which is primarily composed of sodium p-[(4,6-dichloro-1,3,5-triazin-2-yl)amino]benzenesulfonate, the organophosphine tanning agent from Solvay in Belgium, and the organopolymer tanning agent (TWS) from Tingjiang, Sichuan, China, with carboxylic acids, amino acids, and aldehydes as the main functional groups.[21] However, the advancement of wet finishing materials suitable for organic chrome-free tanning systems remains notably lagging.[22] The primary obstacle in developing wet-finishing materials for organic chrome-free tanning systems lies in the interaction between tanning molecules and the amino groups of leather collagen, which diminishes the positive charge of the leather. This reduction in chemical binding sites hampers the absorption and binding rates of traditional anionic wet-finishing materials,[23,24] making them unsuitable for modern tanning system requirements. Amphoteric polymers can enhance the absorption and binding of chemicals during processing by modulating the electrical characteristics of leather substrates.[25–27] The synthesis of on-demand multifunctional amphoteric polymers of the red, green and blue primary colors by structural design based on the principle of the three primary colors can lead to materials capable of full-spectrum color rendering,[28] with the potential to develop a comprehensive solution for leather manufacturing. This innovation could lead to the production of multifunctional materials suitable for tanning, retanning, fatliquoring, and multi-color dyeing to effectively simplify the leather manufacturing stages to meet market demands and deliver substantial environmental benefits.

Leather products occupy an important position in the high-end market; however, they are susceptible to illegal activities, such as the substitution of inferior materials for genuine leather, to the detriment of consumers. Whilst temperature- or light-sensitive dyes have been widely used in textiles such as smart textiles,[29] information encryption,[30] anti-counterfeit labelling[31] and aesthetic design,[32] their use in leather products is still relatively limited and little reported in the existing literature. This provides an important opportunity for the leather industry to further explore and develop these materials. Concurrently, the integration of multifunctional chemical additives containing fluorescent groups can confer fluorescence recognition properties to leather.[33] By combining these fluorescence properties with temperature- or light-sensitive dyes, unique patterns, barcodes, QR codes and other anti-counterfeiting markings can be created.[34,35] These strategies not only enhance the aesthetics of leather products, but also increase their security and authenticity.

The development of chrome-free tanning technology and the modernization of traditional multi-step tanning processes have become a necessity for achieving leather eco-manufacturing evolution. Here, we propose a "one-for-all" strategy through free radical polymerization and amidation grafting reactions to impart multifunctional amphoteric polymers (AADs) with tanning, wet-finishing, and anti-counterfeiting properties to streamline tannery processes and leather chemicals from the origin. The covalent bonding and multi-point crosslinking of AADs with collagen fibers result in crust leather that exhibits values of T_s exceeding 77 °C, excellent physical, mechanical and organoleptic properties, and high resistance to washing and rubbing, surpassing the performance of many existing leather chemical materials. Additionally, the fluorescence properties of AADs allow for the visualization of mass transfer processes and the incorporation of anti-counterfeiting features in leather products, ensuring their authenticity. The implementation of this system leads to a 49.3–58.8% reduction in adverse environmental effects. The "one-for-all" multifunctional materials effectively address the challenges posed by excessive chemical dosages, protracted processing times, and pollutant-laden wastewater discharge inherent to traditional tanning procedures (Fig. 1).

2. Materials and methods

2.1. Materials

Acrylic acid (AA, 99%), allyl glycidyl ether (AGE), hexadecyl dimethylallyl ammonium chloride (DMAAC-16), Reactive Red 180, Reactive Blue 19, 1,8-naphthalimide, dimethylamine (40 wt% in H_2O), ethylenediamine, 1-ethyl-3-(3-dimethyl aminopropyl)carbodiimide (EDC, 98.5%), and N-hydroxy succinimide (NHS, 98%) were procured from Shanghai Maclean Biochemical Technology Co., Ltd. Ammonium persulfate and sodium bisulfite were obtained from Tianjin Tianli Chemical Reagent Co., Ltd. Ethanol absolute was supplied by Aladdin Reagent (Shanghai) Co., Ltd. Temperature-responsive dyes and
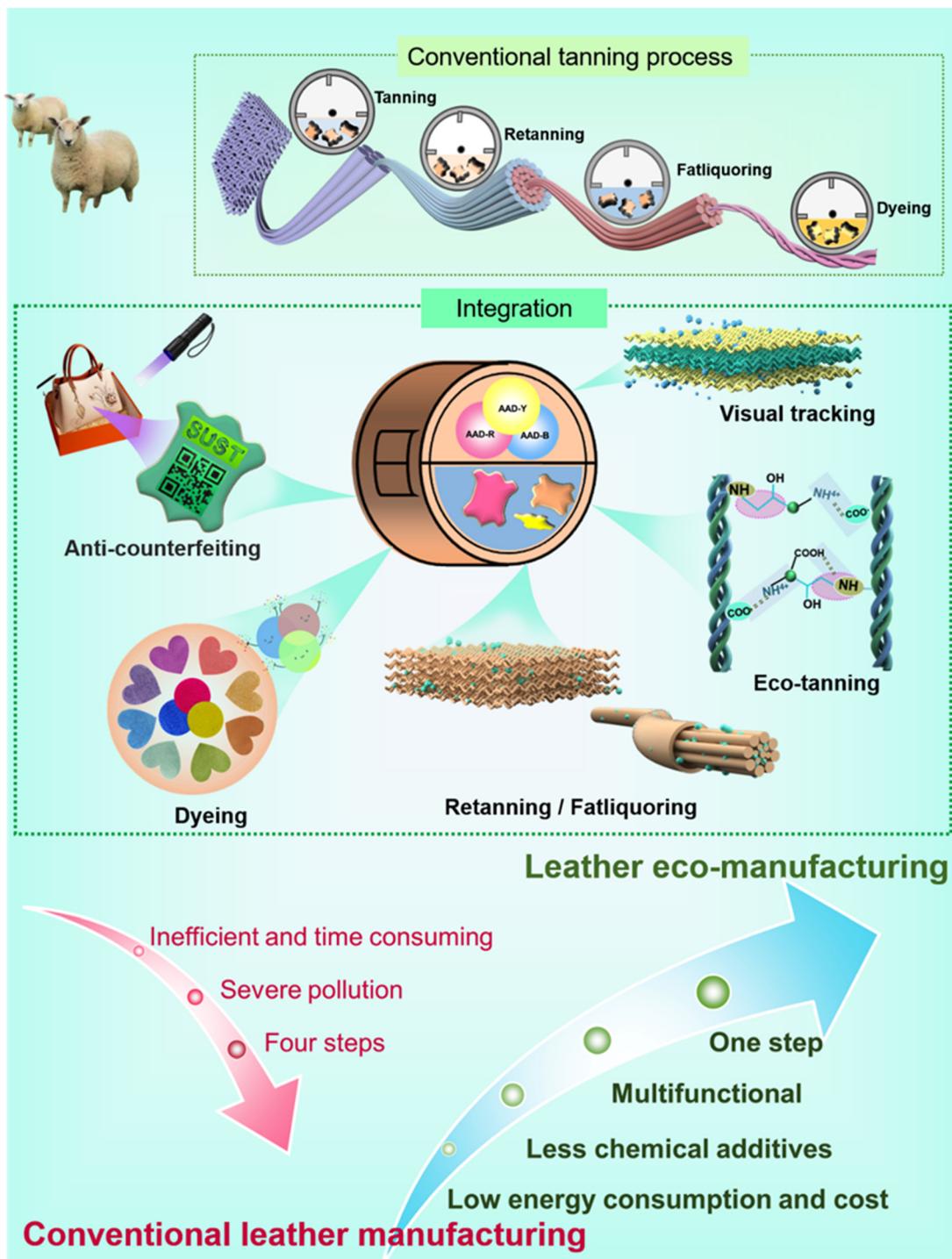
Fig. 1 Schematic illustration of a comparison of the "one-for-all" strategy and the conventional leather manufacturing process.

light-sensitive dyes were sourced from Shenzhen Oriental Color-changing Company. All chemicals were used as received. The TWS tanning agent was supplied by Sichuan Tingjiang New Material Co., Ltd. The F-90 tanning agent was provided by Stahl Leather Chemical Co., Ltd. The AT tanning agent was sourced from Beijing Fanbo Chemical Co., Ltd. Pickled sheepskins were provided by Xinji Ling-Jue Leather Co., Ltd.

2.2. Synthesis of amphoteric polymer tanning agent

The synthetic route for P(AA-AGE-DMAAC16) is illustrated in Fig. 2(a). The cationic monomer DMAAC-16 (0.1 mol, 37.1 g) was placed in a 250 mL three-necked flask equipped with a stirrer and a reflux condenser. Deionized water (40 mL) was added to the flask with continuous stirring at 170 rpm.
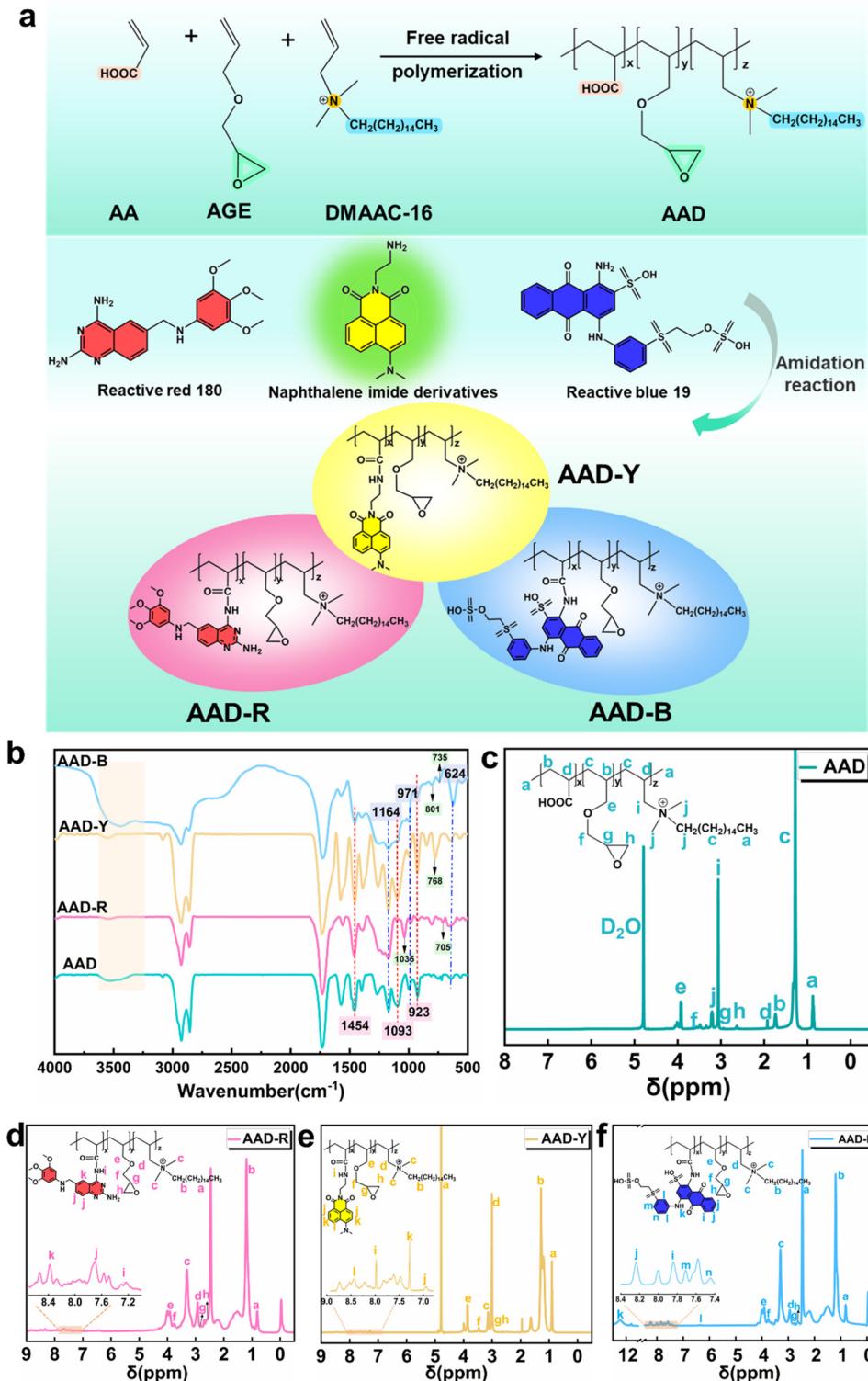
Fig. 2 (a) Synthesis route tfor the amphoteric polymers AAD, AAD-R, AAD-Y, and AAD-B. (b) FT-IR spectra of AAD, AAD-R, AAD-Y, AAD-B. ^{1}H-NMR spectra of AAD (c), AAD-R (d), AAD-Y (e), and AAD-B (f).

Subsequently, allyl glycidyl ether (0.15 mol, 17.1 g) and acrylic acid (0.05 mol, 3.6 g) were added sequentially. An additional 47 mL of deionized water was then introduced, and the pH was adjusted to approximately 6.5. After 15 minutes of stirring,

ammonium persulfate (2.3 g) and sodium bisulfite (0.23 g) were added as initiators. The temperature was gradually increased to 70 °C, and the reaction was maintained at this temperature for 7 hours. Upon completion, the reaction

mixture was purified through recrystallization using acetone. The purified amphoteric polymer, designated as P(AA-AGE-DMAAC16) and abbreviated as AAD, was obtained with a yield of 93.2%.

The synthetic details of AAD-R, AAD-Y, and AAD-B can be found in the ESI.† AAD, AAD-R, AAD-Y, and AAD-B are collectively referred to as AADs. These AADs were utilized in the tanning–wet finishing processes of pickled sheepskins (Table S1†). The dyeing performance and environmental data were compared with leather samples tanned and wet-finished using commercial chrome-free tanning agents (specifically AT, F-90 and TWS) (Tables S2–S5†).

2.3. Characterization

2.3.1 Fourier transform infrared spectroscopy (FT-IR).
AAD, AAD-R, AAD-Y, and AAD-B were analyzed using a Bruker VECTOR-22 Fourier infrared spectrometer employing the potassium bromide (KBr) pellet method. The resolution was set at 4 cm^{-1}, and 32 scans were conducted over a wavenumber range from 500 to 4000 cm^{-1}.

2.3.2 The proton nuclear magnetic resonance hydrogen spectrum (^{1}H-NMR).
AAD and AAD-Y were dissolved in deuterium oxide (D_2O), while AAD-R and AAD-B were dissolved in deuterated dimethyl sulfoxide (DMSO-d_6) to prepare solutions with a concentration of 20 mg mL^{-1}. The samples were then analyzed using a Bruker AVANCE III 600 MHz NMR spectrometer.

2.3.3 Particle size and zeta potential.
AAD, AAD-R, AAD-Y, and AAD-B were dissolved in deionized water to prepare 1 wt% solutions. Following this, the particle size and zeta potential were assessed using a nanoparticle size analyzer within a pH range of 3.0–8.0.

2.3.4 Gel permeation chromatography (GPC).
Nine milligrams of AAD, AAD-R, AAD-Y, and AAD-B were dissolved in 3 mL of deionized water and filtered through a 0.45 μm needle-like membrane. The molecular weight and molecular weight distribution were determined using a Waters 1515 HPLC liquid chromatography system.

2.3.5 Fluorescence imaging.
Pickled sheepskin samples tanned with AAD-Y for different durations (30, 60, 120, 240, 360, and 480 minutes) were analyzed. The penetration process of AAD-Y in the longitudinal section of the leather of the dried samples was observed using a laser confocal microscope.

2.3.6 Pore structure and microstructure.
Pickled sheepskin and leather treated with AAD, AAD-R, AAD-Y, and AAD-B were freeze-dried for 48 hours. The pore structure and pore size distribution of the samples were assessed using an automated mercury porosimeter. The fiber distribution in the longitudinal section of the samples was observed using a field emission scanning electron microscope (FESEM), while the grain surface morphology was examined with a three-dimensional microscope with an ultra-depth field.

2.3.7 Fundamental characteristics of crust leather.
According to the standard (ISO 3380: 2015), the shrinkage temperature of pickled leather treated with AAD, AAD-R, AAD-Y, and AAD-B was determined using a shrinkage tempera-

ture tester (MSW-YD4, Shaanxi University of Science and Technology, China). The dry thermal stability of the leather samples was assessed using a STA449F3-1053-M TGA thermogravimetric analyzer (NETZSCH, Germany). Prior to softness measurement (mm) with a GT-303-D leather softness tester, the leather samples were conditioned at 25 °C and 65% RH for 24 hours. The MH-YDI digital leather thickness tester was employed to gauge the thickness at five points before and after tanning, and the thickness change rate (%) was calculated. The tensile strength (MPa), elongation at break (%), and tear strength (N mm^{-1}) of crust leather were measured using a TH-8203 S tensile testing machine, in accordance with the standard methods (IUP 6, 2000; IUP 8, 2000).

2.3.8 Evaluation of dyeing performance.
Leather samples with different colors were cut into small pieces of 4 cm × 4 cm dimensions. The lightness (L), red–green axis (a), red–blue axis (b), color depth (K/S) and spectral data were detected using a desktop spectrophotometer within the wavelength range of 380–780 nm. The total color variation was calculated using formula (1):

$$\Delta E = \sqrt{(\Delta L)^2 + (\Delta a)^2 + (\Delta b)^2} \tag{1}$$

Among these parameters, ΔE represents color variation, ΔL denotes brightness difference, Δa signifies the red–green index difference, and Δb indicates the yellow–blue index difference.

The color variation of each sample was measured five times concurrently, and the average value was computed. In accordance with the standard (QB/T 2537-2001), the leather sample was cut into a 135 mm × 60 mm rectangular strip and the dry and wet friction resistance of the dyed leather was tested using the leather color fastness tester. The L, a, and b values of the leather before and after friction were tested using a spectrophotometer, and the color difference pre- and post-friction was calculated according to formula (1).

In addition, leather samples of different colors were cut into small pieces measuring 2 cm × 2 cm. Subsequently, these pieces were immersed in 10 mL of deionized water and subjected to a constant temperature of 37 °C in a shock box rotating at 150 rpm for 24 hours. The spectral data of the soaking solution were tested using a Cary 5000 model ultraviolet–visible spectrophotometer, and the alterations in the color of the leather samples before and after soaking were observed.

2.3.9 Analysis of the wastewater environment.
The tannery waste liquid, both before and after tanning–wet finishing, was collected and diluted by a specific factor. The total organic carbon (TOC) was analyzed using a total organic carbon analyzer to assess the absorption rate, which was determined by the TOC variation pre- and post-tanning. The chemical oxygen demand (COD) of the wastewater was tested according to the standard (HJ/T399-2007), while the biochemical oxygen demand (BOD_5) in the collected tanning wastewater was determined using a biochemical oxygen demand meter (BOD Tral II Hach).

2.3.10 Life cycle assessment. The life cycle assessment (LCA) analysis was conducted using an OpenLCA 2.2.0 in compliance with the ISO 14040 standard. The objective of the study was to compare the environmental impacts of the integrated tanning process with two chromium-free tanning multistep processes. Functional units were defined to represent the production of one ton of sheep pickled hide.[36,37] The system boundary included the tanning process and wet-finishing process. Specific impact categories from CML v4.8 2016 and EF v3.1 were selected for the environmental impact assessment, such as primary energy demand (PED), abiotic depletion potential (ADP), water use (WU), global warming potential (GWP), acidification potential (AP), eutrophication potential (EP), freshwater ecotoxicity (ET), human toxicity cancer effects (HTC) and human toxicity noncancer effects (HTNC). The detailed process of LCA is shown in Fig. S1–S6.†

3. Results and discussion

3.1. Structural analysis of AAD, AAD-R, AAD-Y, and AAD-B

Amphoteric polymer AAD was synthesized *via* free radical polymerization using AA, AGE, and DMAAC-16 as monomers, followed by amidation reactions to produce AAD-R, AAD-Y, and AAD-B (Fig. 2(a)). As depicted in Fig. 2(b), the characteristic absorption peak at 1164 cm^{-1} corresponds to the N–C stretching vibration in the DMAAC-16 monomer, while the peak at 971 cm^{-1} is attributed to the quaternary ammonium group,[38] and the peak at 624 cm^{-1} corresponds to the N–C bending vibration. The –CH$_2$ bending vibrational absorption peak at 1454 cm^{-1} is bonded to the nitrogen cation.[39] The absorption peak at 1093 cm^{-1} is indicative of the presence of the ether bond (C–O–C) in the AGE monomer, and the peak at 923 cm^{-1} is characteristic of the epoxy group.[40] Notably, the absence of an absorption peak at 1640 cm^{-1}, associated with the C=C bond, indicates the complete reaction of the monomers without residual monomer in the polymer. Additionally, the ^{1}H-NMR spectrum in Fig. 2(c–f) displays chemical shifts at 0.86 ppm corresponding to the protons in the –CH$_3$ structure in the main chain, 1.22 ppm and 1.72 ppm corresponding to the protons in the –CH$_2$– structure in the main chain, and 1.91 ppm corresponding to the proton of the tertiary hydrogen atom connected to the tertiary carbon atom in the main chain.[41] Peaks at 3.04 ppm and 3.18 ppm are assigned to the protons in –CH$_3$ and –CH$_2$– groups connected by N$^+$, respectively,[42] while peaks at 2.79 ppm and 2.91 ppm are assigned to the protons in the alkyl groups connected to the O atom in the epoxy group.[43] Peaks at 3.47 ppm and 3.91 ppm correspond to the protons in the –CH$_2$– groups on both sides of the O atom in the ether bond. The chemical shift of the protons in –CH$_2$– connected to the main chain and O is influenced by both the epoxy group and the ether bond, resulting in a higher chemical shift, appearing in the highest field.[44] The absence of peaks beyond 5 ppm in the AAD ^{1}H-NMR spectrum confirms the absence of protons in double bonds. Furthermore, the FT-IR and ^{1}H-NMR spectra of AAD-R, AAD-Y, and AAD-B did not exhibit any amino peaks, and the characteristic peaks of Reactive Red 180, DMENA, and Reactive Blue 19 were observed, confirming the successful synthesis of AAD-R, AAD-Y, and AAD-B.

The relative molecular mass, particle size distribution, and electrical properties of zwitterionic polymers together determine their penetration ability, bonding strength, and final leather properties in leather. Amphoteric polymer molecules with a relative molecular mass between 500 and 3000 Da can effectively crosslink with collagen fibers.[45] Those with a relative molecular mass exceeding 3000 Da can fill in the three-dimensional network structure of leather, enhancing its fullness and elasticity.[46] As illustrated in Fig. 3(a), the number-average molecular weights of AAD, AAD-R, AAD-Y, and AAD-B fall predominantly within the 1000–3000 Da range, indicating their ability to penetrate collagen fibers and achieve effective crosslinking. The smaller emulsion particle sizes of the amphoteric polymer correspond to better permeability. An average emulsion particle size below 500 Da and a polydispersity index (PDI) less than 0.5, as depicted in Fig. 3(b), suggest relatively stable and uniformly distributed emulsion, facilitating rapid and uniform penetration into the leather collagen fibers for superior tanning effects.[47] Fig. 3(c) illustrates that the charge type and magnitude of AAD, AAD-R, AAD-Y, and AAD-B vary with variations in pH. As the pH increases from 3 to 8, the charge type transitions from positive to negative, and the zeta potential initially decreases and then increases, confirming the amphoteric nature of these polymers. Additionally, the isoelectric points of these polymers are all greater than 6, indicating that they are positively charged under mildly acidic conditions. This property enhances the isoelectric point of the treated leather collagen fibers, thereby improving the absorption rate of subsequent anionic dyeing and finishing materials.[48]

3.2. Penetration and dispersion of AADs in leather

The utilization of the fluorescent tracer method has been proved to be an effective technique for characterizing the penetration dynamics of integrated amphoteric polymers within leather materials. In this study, the naphthalimide fluorescent dye DMENA was grafted onto the side chain of the amphoteric polymer, and its distribution within the leather was monitored using a fluorescence microscope to investigate its penetration behavior and underlying mechanisms. The results shown in Fig. 4(a) and (b) illustrate that the integrated amphoteric polymer exhibits a uniform pattern of penetration into the collagen fibers after a duration of 480 minutes, primarily entering from the flesh side of the leather.[49] Furthermore, the data suggest that prolonged treatment durations lead to deeper penetration and better dispersion of collagen fibers. This observation aligns with the analysis of leather porosity, which shows a significant increase in porosity and average pore size in leather samples treated with AAD, AAD-R, AAD-Y, and AAD-B in comparison with PS-treated leather (Fig. 4(c–g)). The pore size distribution of the treated leather ranges from 100 to 3000 nm (Fig. 4(h)), indicating that the integrated amphoteric
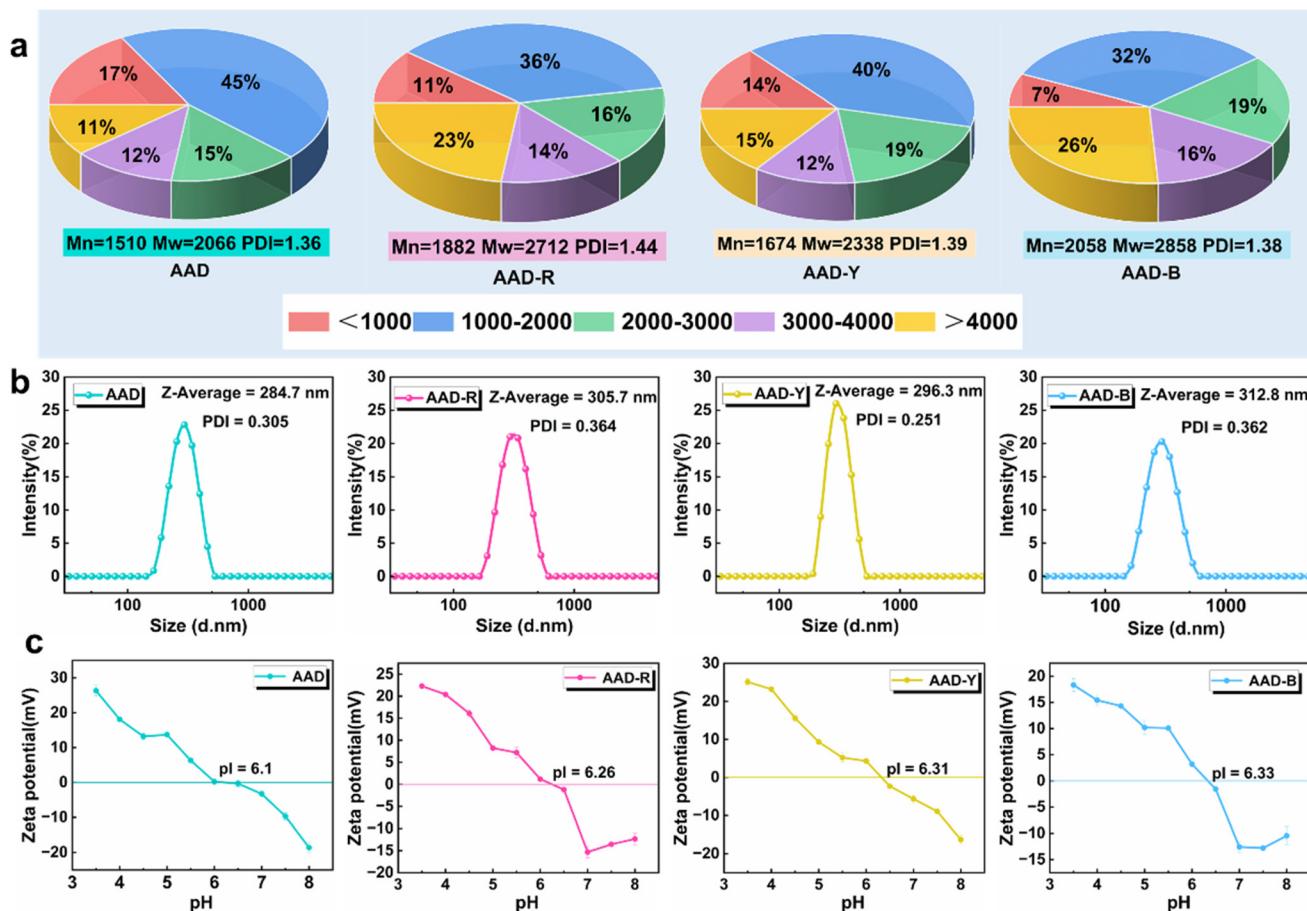
Fig. 3 (a) Molecular weight distribution, (b) particle size and (c) zeta potential of AAD, AAD-R, AAD-Y and AAD-B.

polymer, characterized by its relatively small molecular mass and emulsion particle size, can effectively penetrate the micron and submicron size pores present within the collagen fibers.[50]

The collagen matrix is composed of different levels of fibers, and its structural characteristics play a crucial role in determining the quality of leather (Fig. 5(a)). Achieving good dispersibility is crucial for improving the physical properties, ensuring uniform tanning, and enhancing the overall quality of leather.[51] Amphoteric polymers with low molecular weight and linear or branched structures have the ability to easily diffuse and distribute within the collagen fiber network. FESEM images reveal that collagen fibers in PS are interconnected due to strong hydrogen bonding between polar groups on the collagen side chains, resulting in the formation of thin and brittle fibers upon drying (Fig. 5(b)). In contrast, when the AAD amphoteric polymer evenly infiltrates the leather, it increases the porosity of the fiber matrix and significantly enhances the thickness of the longitudinal section. This treatment results in leather that is more flexible, extensible, and elastic after drying. The long alkyl chain in the AAD structure aids in separating bonded collagen fibers, facilitating the sliding of adjacent collagen fiber bundles relative to each other, and thereby promoting highly dispersed fibers.[52] The epoxy group, quaternary ammonium ion, and carboxyl group

in the molecular structure can establish multi-point binding with the active groups of collagen fibers through covalent bonds, electrostatic adsorption, and hydrogen bonding, thereby improving structural stability.[53] Upon post-treatment with the amphoteric polymer, the leather retains the D-periodic structure of collagen fibers, with an approximate periodicity of 65 nm, indicating that the microstructure of collagen fibers remains intact.[54] The enhanced dispersion of collagen fibers by AAD creates clear and orderly pores on the grain surface (Fig. 5(c and d)), significantly improving the air permeability and water vapor permeability of the leather, thereby increasing its practical value.

3.3. Tanning–retanning–fatliquoring performances of AADs

Fig. 6(a) illustrates the dispersion, filling, lubrication, and crosslinking mechanisms of the integrated amphoteric polymer on collagen fibers. The amphoteric polymer molecules of AAD contain side chains with epoxy groups, positively charged quaternary ammonium ions, carboxyl groups, and long flexible alkyl chains. These active groups interact with the amino, carboxyl, and hydroxyl groups present in collagen fibers, thereby enhancing the structural stability of the fibers through covalent bonding, hydrogen bonding, electrostatic adsorption, and other mechanisms[55](Fig. S7†). Compared to
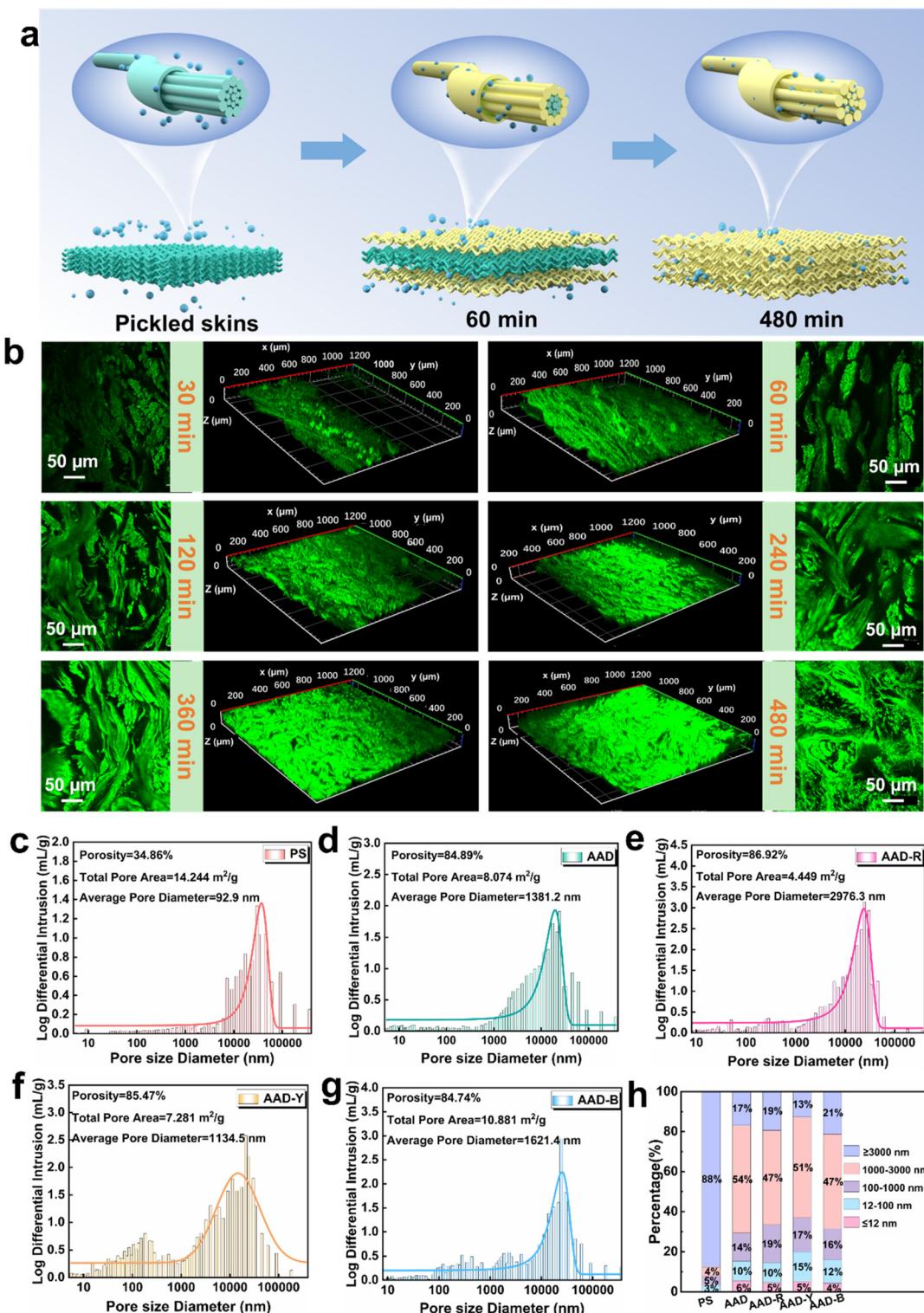
Fig. 4 (a) Penetration process diagram of AADs in leather. (b) Fluorescent images of different penetration times (30, 60, 120, 240, 360, and 480 min) of integrated amphoteric polymers in leather (Ex = 488 nm and Em = 545 nm). Pore structure and pore diameter distribution of PS (c), AAD (d), AAD-R (e), AAD-Y (f), and AAD-B (g) treated leather. (h) Percentage of pore diameter distribution of different leather samples.

PS, leather treated with AADs exhibited a significant increase in the shrinkage temperature by 33.1–35.3 °C (Fig. 6(d)), an increase in the maximum thermal decomposition temperature

of 8–12 °C, and a higher carbon residue upon complete degradation, indicating a substantial improvement in thermal stability[56] (Fig. 6(b and c)). Furthermore, the long alkyl chains in
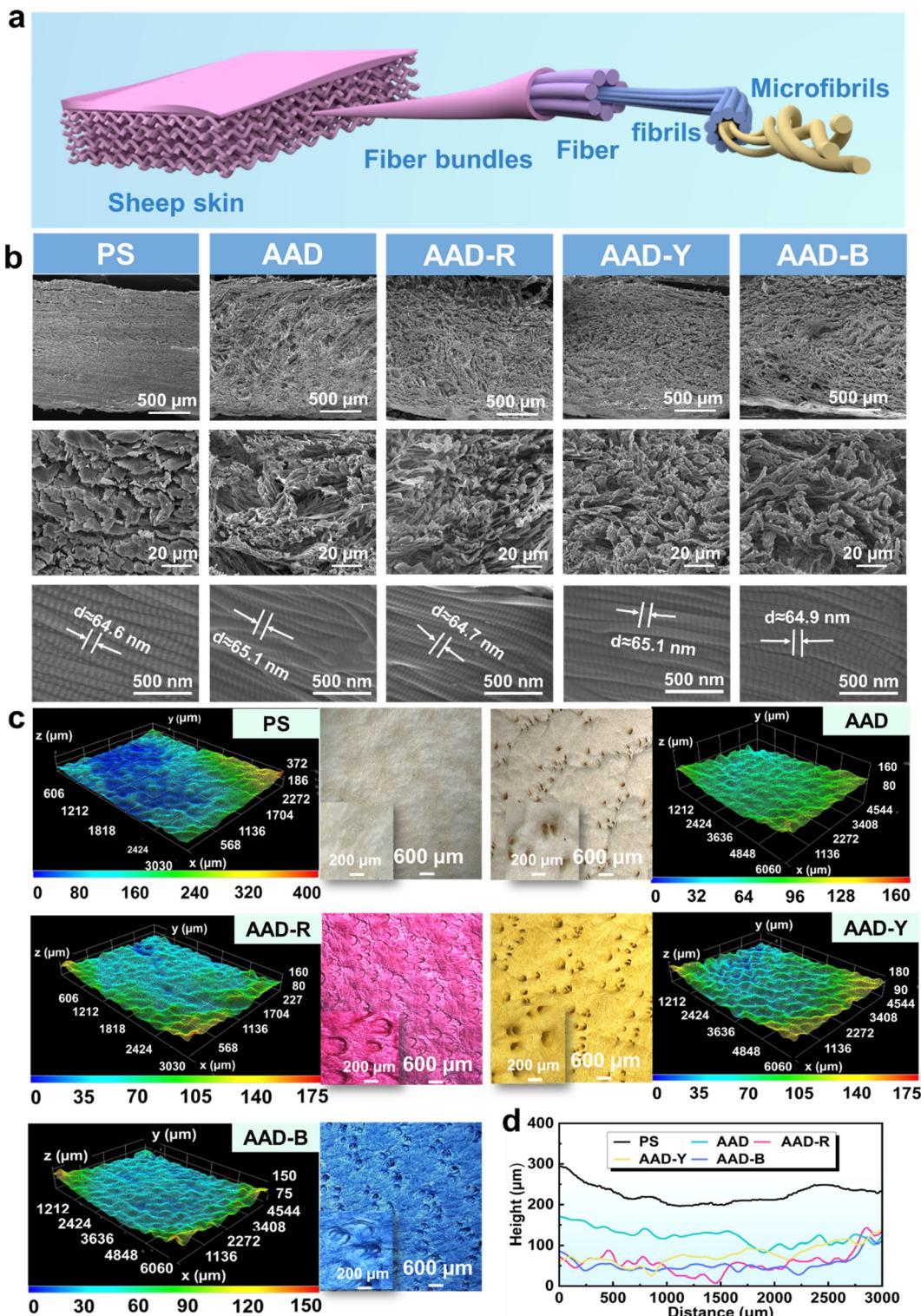
Fig. 5 (a) Multi-layered structure of collagen fibers. FESEM images (b) and grain surface micro-morphology (c) of PS and AAD, AAD-R, AAD-Y, and AAD-B treated leather samples. (d) Surface morphology fitting curves of different leather samples.

the AAD structure facilitate relative slip among collagen fibers within the fiber matrix. This action fills the gaps within the loosely woven collagen fiber bundles, thereby enhancing the flexibility and fullness of the leather (Fig. 6(e and f)).

Consequently, unlike chrome-free tanning agents, which only offer tanning capabilities, the AADs, with their integrated tanning–retanning–fatliquoring functions, endow the leather with superior softness, tensile strength, tear strength, and
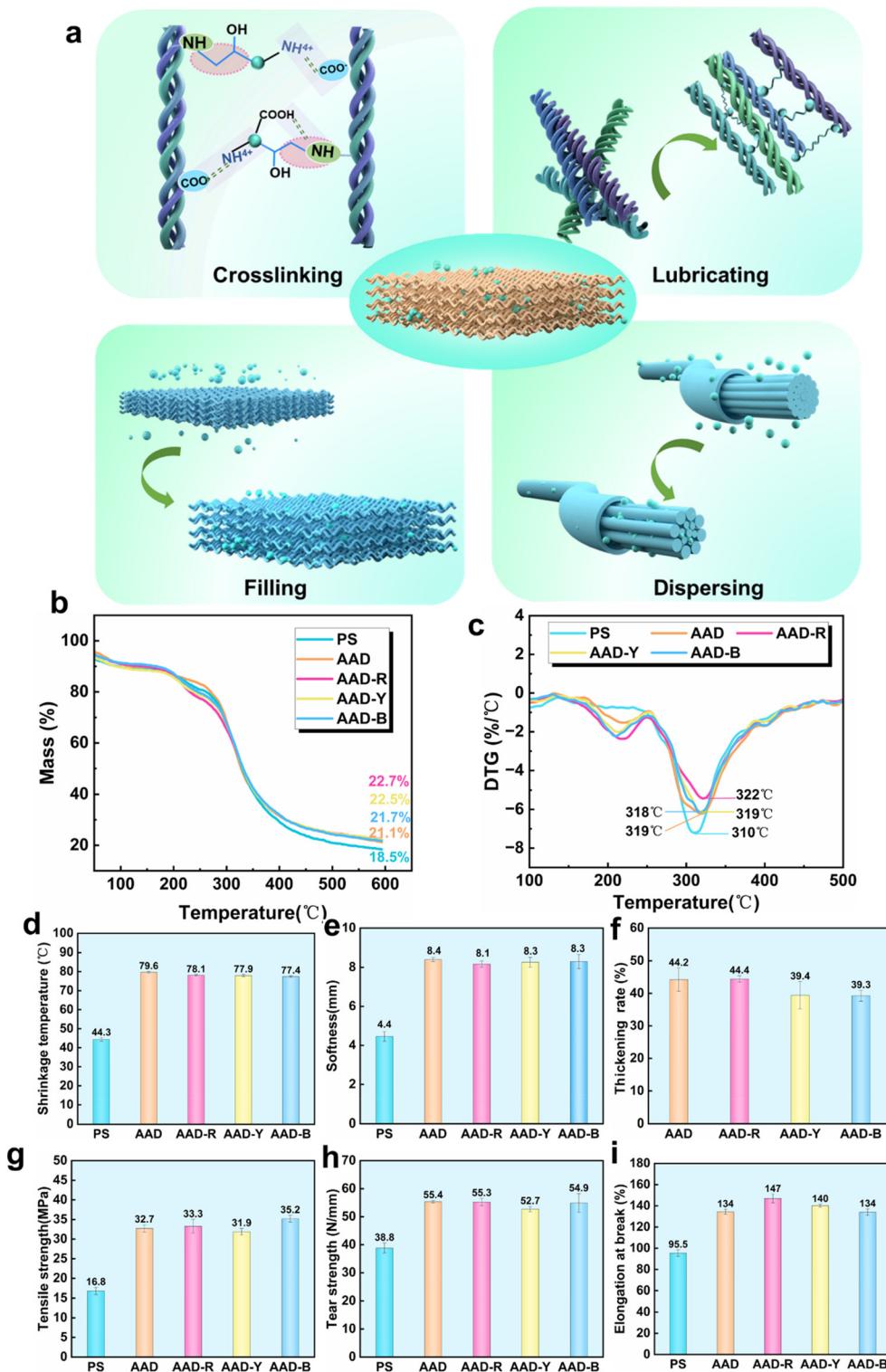
Fig. 6 (a) Schematic diagram of dispersion, filling, lubrication and crosslinking of AADs in leather. (b) TG curves, (c) DTG curves, (d) T_s, (e) softness, (f) thickening rate, (g) tensile strength, (h) tear strength, and (i) elongation at break of different leather samples.

elongation at break (Fig. 6(g–i), Fig. S8† and Table 1). These combined properties surpass those of most tanning agents currently under study and meet the standards specified in the Chinese Garment Leather Standard (QB/T 1872-2004).

3.4. Dyeing performances of AADs

The three primary color amphoteric polymers, AAD-R, AAD-Y, and AAD-B, can be combined in varying proportions to

Table 1 Comparison of fundamental properties between AAD treated leather and typical tanning agent tanned leather
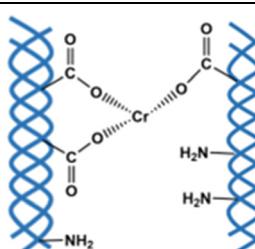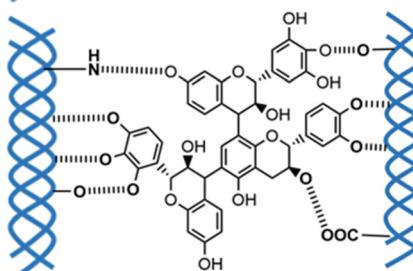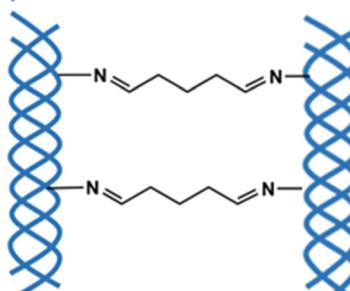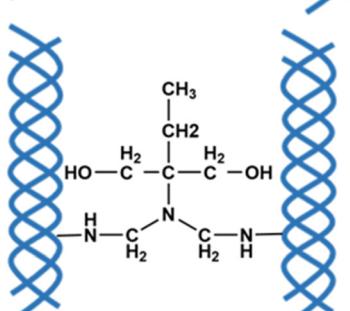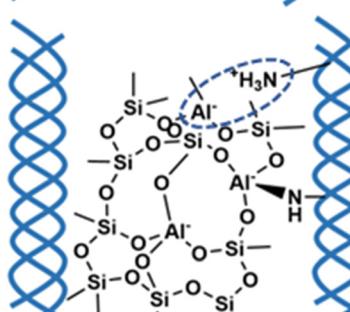
| Tanning agents	Classification	Reaction schemes	Shrinkage temperature (°C)	Tensile strength (MPa)/elongation (%)/tear strength (N mm^{-1})	Ref.
Basic chromium sulphate (BCS)	Chrome tanning agent		102	29.4/57/66	57
Tannic acid	Vegetable tanning agent		70.0	36.0/33.0/76.0	58
Glutaraldehyde	Aldehyde tanning agent		85	18.0/56.0/n/a	59
Oxazolidine	Synthetic organic tanning agent		77	16/76/n/a	60
Zeology	Inorganic tanning agent		74.9	n/a	61

Table 1 *(Contd.)*
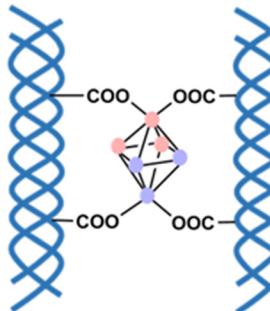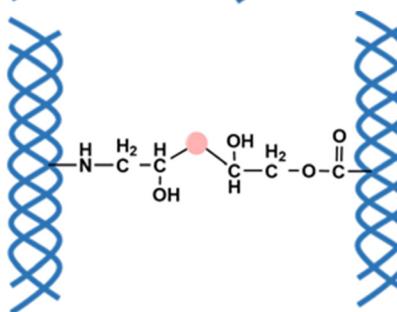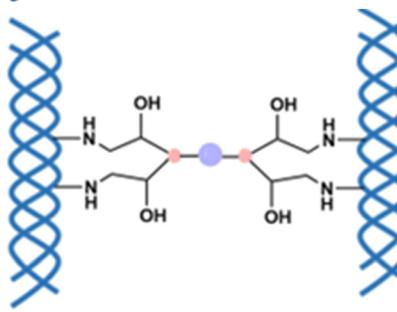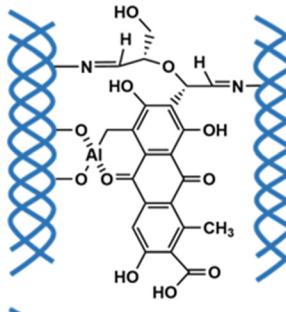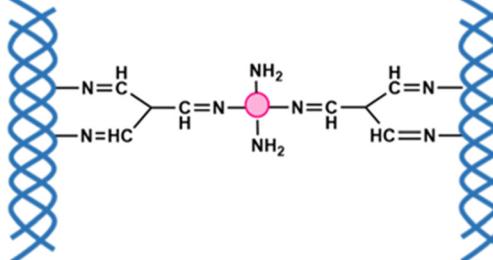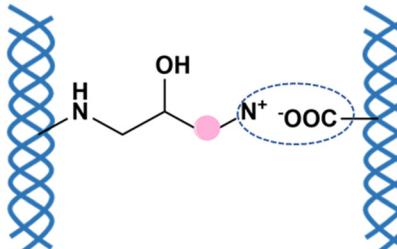
| Tanning agents	Classification	Reaction schemes	Shrinkage temperature (°C)	Tensile strength (MPa)/elongation (%)/tear strength (N mm^{-1})	Ref.
Zr/M-MOFs	Inorganic–organic hybrid tanning agent		79.9	16/55/35	62
COS-GTE	Bio-based tanning agent		83.5	10.1/62.6/47.4	14
HHTT-EGDE-CP	Bio-based tanning agent		78.7	13.5/68.2/54.2	63
CCDA	Bio-based tanning agent		70	13/70/54	23
DCMC	Bio-based tanning agent		80.0	12.7/n/a/28.8	64

Table 1 (Contd.)

| Tanning agents	Classification	Reaction schemes	Shrinkage temperature (°C)	Tensile strength (MPa)/elongation (%)/tear strength (N mm^{-1})	Ref.
AADs	This work		79.6	32.7/134/55.4	—

produce an integrated material encompassing a complete chromatic range. As illustrated in Fig. 7(a), the dyed leather exhibited a spectrum of colors, including red, orange, yellow, green, cyan, blue, and purple. The longitudinal section of the dyed leather presented in Fig. S9† demonstrates that the AADs can uniformly penetrate into the interior of the leather's collagen fibers, effectively coloring the material. The incorporation of the naphthalimide derivative in the molecular structure of AAD-Y imparts the dyed leather with yellow, yellow-green, green, and cyan fluorescence under ultraviolet light, enhancing the aesthetic and anti-counterfeiting properties of leather products. Fig. 7(b) presents full-color dyed leather samples prepared by simply mixing different proportions of the trichromatic amphoteric polymers. The CIE coordinates, derived from the spectral data of the dyed leather, indicate more pronounced color changes. The circular region defined by the coordinates (0.46, 0.25), (0.40, 0.44), and (0.19, 0.16) in Fig. 7(c) represents the achievable color gamut for AAD-R, AAD-Y, and AAD-B. Fig. 7(d) and (e) show that the surface color of the dyed leather is both dark and uniform.

Fig. 7(f–h) illustrates the difference in color fastness between leather dyed with the integrated material and leather dyed with traditional anionic dyes. As observed in Fig. 7(f), both types of dyed leather demonstrate similar dry rubbing fastness. However, the wet rubbing resistance of organically tanned leather (TWS, F-90, AT) dyed with traditional anionic dyes is significantly lower compared to that of leather dyed with integrated materials (Tables S6 and S7†). Notably, in terms of washing resistance, the color of the integrated material-dyed leather surface remains nearly unchanged after soaking and five cycles of washing in water (Fig. S10†) and the dyed leather samples achieve a wash fastness rating of 4 or higher (Table S8†). In contrast, the color of the anionic dye-treated surfaces lightened considerably. Specifically, the dyes on the F-90 and AT-tanned leather surfaces were almost completely exfoliated (Fig. 7(h)), and the absorbance of the soaking solution approached 1 (Fig. 7(g)). This disparity is primarily attributed to the different binding mechanisms between the integrated material and the traditional anionic dyes with collagen fibers. AADs form covalent bonds with collagen fibers, whereas anionic dyes rely on electrostatic interactions and hydrogen bonding. The presence of water molecules can disrupt the original hydrogen bonds between dye molecules and fibers by establishing new hydrogen bonds with amino and carboxyl groups on collagen fibers.[23] Additionally, water molecules can significantly weaken or break the electrostatic interactions between negatively charged dyes and positively charged collagen fibers through their polarity, solubility, and ion separation effects. Covalent bonds, being much stronger than hydrogen bonds and electrostatic interactions, are generally resistant to disruption by water molecules.[24] Overall, the color fastness of leather is significantly enhanced when it is dyed with integrated materials, effectively addressing the "long-standing problem" of poor wash resistance in traditionally dyed leather.

3.5. Anti-counterfeiting performances of AADs

The integration of effective anti-counterfeiting technology in the leather industry is essential for its sustainable growth. This research introduces a novel anti-counterfeiting design for leather that reacts to temperature, light, and a combination of both. This is achieved through the vacuum filtration method and the surface brushing and coating method (Fig. 8(e)). As shown in Fig. 8(a) and (c), the *Ginkgo biloba* and "SUST" patterns remain invisible under natural light at temperatures below 37 °C. However, when the temperature exceeds 37 °C due to external heating, human touch, or exposure to 365 nm ultraviolet light, these patterns become visible against the base color of the leather. Conversely, the clover-shaped pattern shown in Fig. 8(b) remains invisible at temperatures above 37 °C but becomes visible under lower temperatures or UV light exposure. This innovative approach can be utilized to incorporate anti-counterfeiting measures into high-grade leather products, improving their visual appeal and providing consumers with a trustworthy method to authenticate genuine products.

Barcodes and QR codes have become essential tools for modern information exchange due to their convenience and versatility.[65,66] As illustrated in Fig. 8(d), the design of barcodes and QR codes can be integrated into leather products, allowing for the direct retrieval of product information
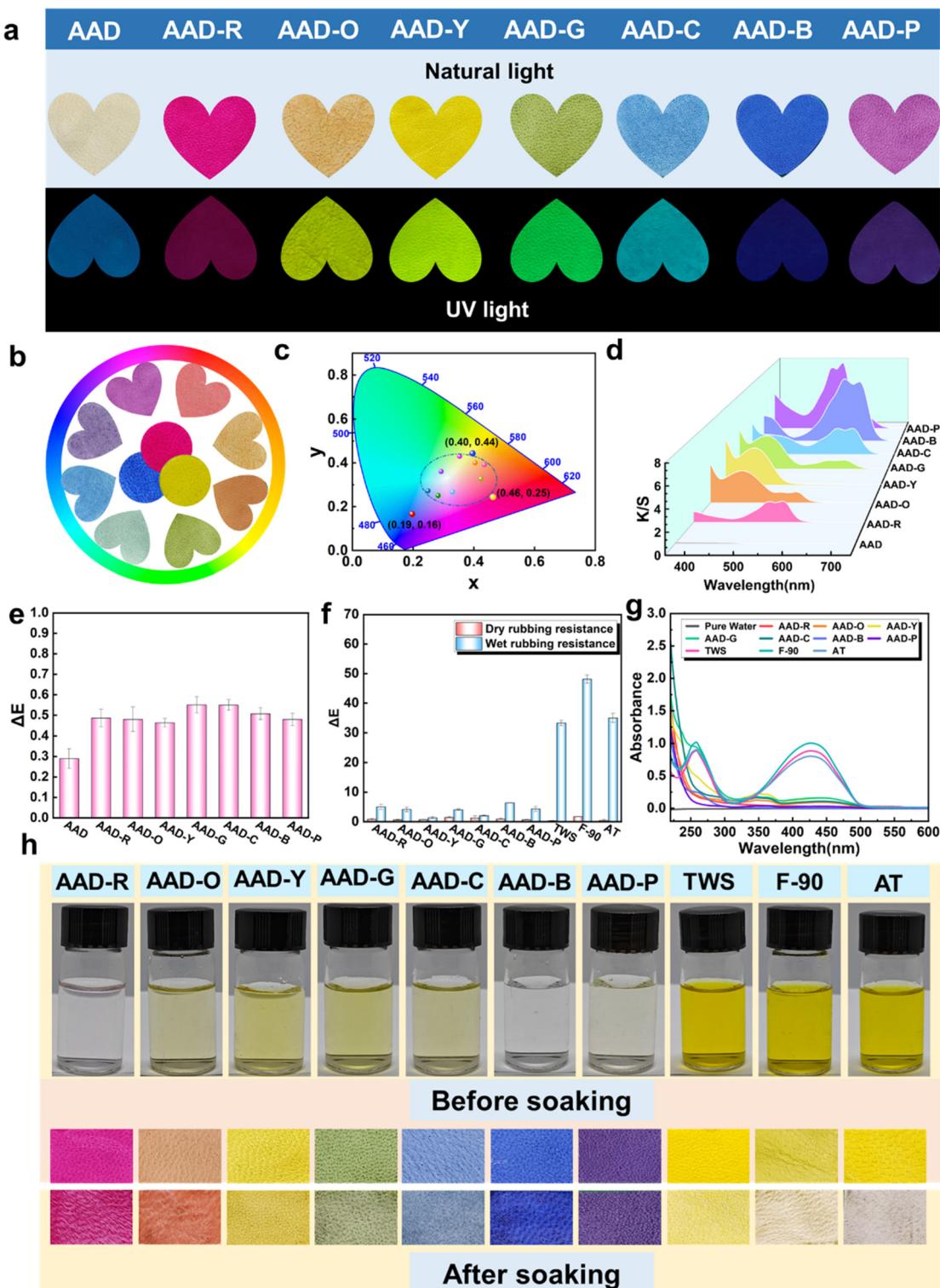
Fig. 7 (a) Optical photographs of leather surfaces dyed with AAD-R–AAD-P under natural light and ultraviolet light. (b) Full-spectrum dyeing and (c) dyed leather CIE coordinates of trichromatic amphoteric polymer after mixing. (d) *K/S* value and (e) dyeing uniformity of leather dyed with AAD-R–AAD-P. (f) The wet and dry rubbing resistance, (g) UV-vis spectra of the soaking solution, and (h) leather surface before and after soaking of different dyed leather samples.

Fig. 8 *Ginkgo biloba*, clover, SUST shape temperature-response (a), temperature–light double response (b), and light-response (c) leather anti-counterfeiting pattern. (d) Temperature–light response leather barcode, and QR code anti-counterfeiting pattern. (e) The production method of the leather anti-counterfeiting pattern. (f) Application scenario diagram of leather anti-counterfeiting patterns.

through scanning with a mobile phone (Genuine Leather Product, GLP). To further enhance the confidentiality of product details, these QR codes remain invisible at low temp-

eratures and under natural light. Consumers can reveal the patterns by applying heating or exposing them to UV light, and then scanning the code to verify product security information

(Fig. 8(f)). This method of direct identification and information encryption offers a more secure and reliable option compared to traditional techniques, such as tactile inspection for authenticating leather products. This technological advancement positively impacts consumer trust in leather products and promotes the benign development of the market.

3.6. Environmental impact analysis

Environmental impact plays a significant role in constraining sustainable development of the current leather industry.[67] The integrated tanning–wet finishing processes, as shown in Table S9,† utilizes fewer types and smaller amounts of additives compared to the traditional multi-step tanning process, resulting in a significant reduction in processing time from 1095–2360 min to 500 min. Additionally, it decreases leather-chemical usage by 47.5–74.8% and reduces water consumption by 82.6–90%. Furthermore, as presented in Table S10,† the material absorption rate in the multi-step processing technology is substantially lower than that in the integrated process. This discrepancy is primarily due to the insufficient positive

charge on the leather after tanning with TWS, F-90, and AT organic tanning agents. During the wet finishing process, the binding rate of anionic retanning agents, fatliquors, dyes, and collagen fibers is low, leading to the unbound wet finishing aids remaining in the tanning wastewater and increasing its COD and BOD (Table S11†). The BOD/COD ratio below 0.3 indicates poor biodegradability, highlighting the detrimental environmental impact.[68,69]

A life cycle assessment was conducted to compare the environmental impact of integrated technology and multi-stage technology in processing 1 ton of sheepskin. This assessment evaluated resource consumption, climate change, ecosystem quality, and human health effects during the production processes. The LCA results in Fig. 9 show that the environmental impact of AADs is 49.3% and 58.8% lower than those of SACG and EHBP systems respectively, indicating the superior environmental performance of the AAD system (Tables S12–S14†). Traditionally, ecotoxicity and human toxicity are key concerns in leather manufacturing. However, the AAD tanning–wet finishing integration process shows extra-
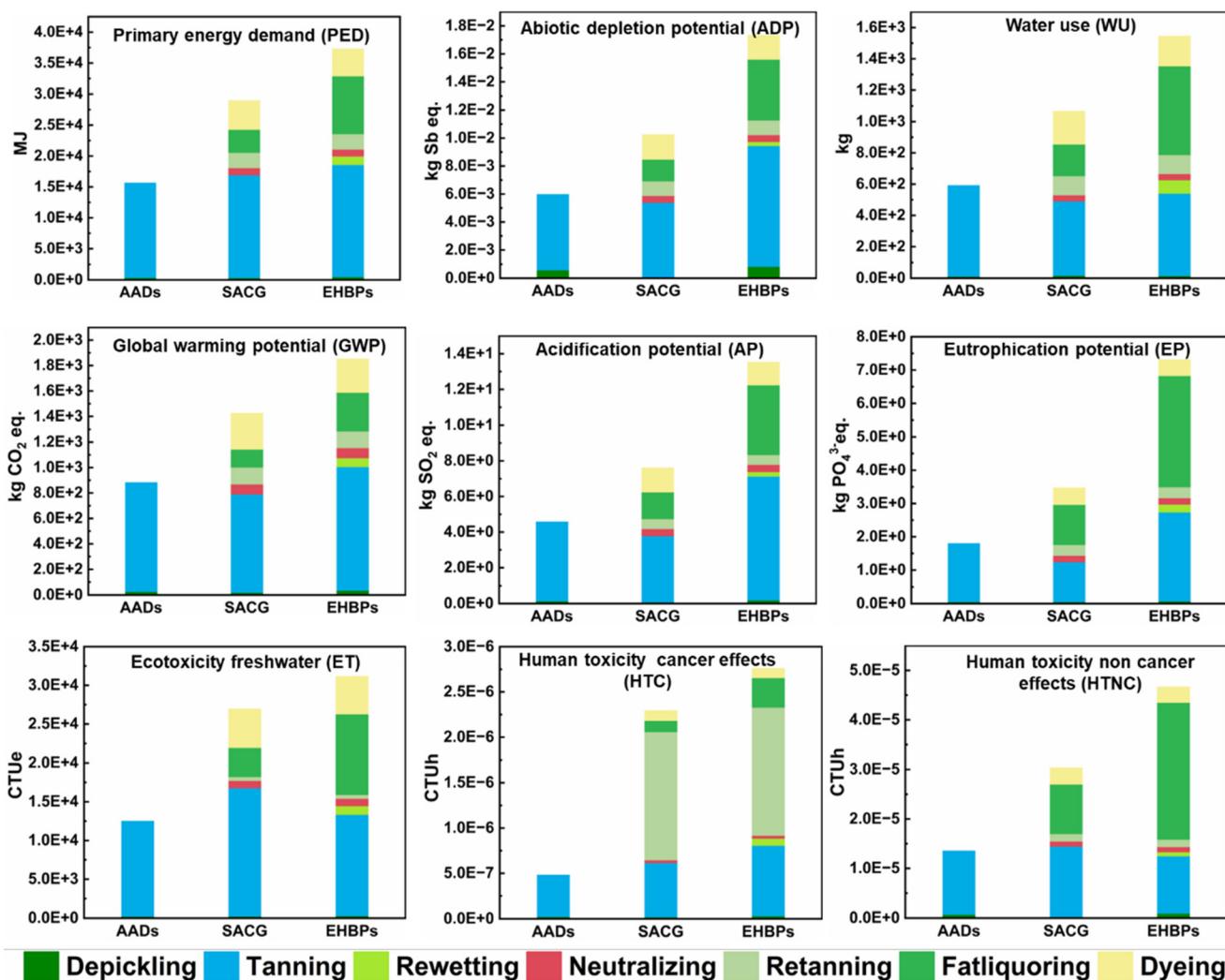

Fig. 9 Comparison of environmental impact parameters of AADs, EHBPs, and SACG.

ordinary performance. For example, compared to the EHBP system, the HTC and HTNC are decreased by 82.6% and 71%, respectively, demonstrating that reducing the use of chemical additives in the tanning process reduces human toxicity.

From the standpoint of resource and cost efficiency, the integrated process ensures efficient resource utilization and reduces the carbon footprint of the production process by lowering energy consumption.[21,70] The examination of tannery wastewater highlights the environmental friendliness of the integrated process, reducing the environmental repercussions associated with production. Therefore, when compared with the traditional multi-step tanning process, this method aligns well with the principles of green chemistry and sustainable manufacturing, offering a promising alternative to traditional tanning processes.

4. Conclusions

In summary, we developed a facile and energy-efficient "one-for-all" strategy to streamline multiple leather processing stages, enhancing the ecological viability of chrome-free tanning technologies through on-demand multifunctional amphoteric polymers, AADs. AADs were synthesized *via* free radical polymerization and amidation reactions in aqueous environments for integrating the marvelous multi-functionalities of tanning, retanning, fatliquoring, regulable color-dyeing, and anti-counterfeiting marking. Leather treated with AADs exhibited a shrinkage temperature exceeding 77 °C, along with enhanced softness, tensile strength, and elongation at break compared to the leather processed through the conventional multi-step methods, showcasing the excellent tanning and wet-finishing performance of the one-step method. The cross-linking through the covalent bonding between AADs and collagen fibers imparts AAD-dyed leather with exceptional resistance to rubbing and washing. Leveraging the fluorescent properties of AADs, the visualization of the mass transfer process in leather is realized, and combined with light-/heat-sensitive dyes, distinctive patterns, barcodes, QR-codes, and other anti-counterfeiting markers can be created in leather products. Remarkably, by consolidating multiple primary processes (tanning, retanning, fatliquoring, and dyeing) into one single process, this approach resulted in a significant reduction of 57–71.6% in human-health impacts and a reduction of 38.2–52.4% in greenhouse gas emissions. The "one-for-all" process also prominently decreases the environmental impact categories by 49.3–58.8% compared to traditional multi-stage methods, thereby reducing the carbon and environmental footprint of leather production. The approach provides a sustainable and eco-friendly solution for tanning processes, steering the leather industry towards more environmentally conscious practices.

Author contributions

Chao Wei: methodology, data curation, writing – original draft, and writing – review & editing. Xuechuan Wang: investigation,

funding acquisition, and supervision. Shuang Liang: software and methodology. Xiaoliang Zou: software. Long Xie: validation. Xinhua Liu: conceptualization and supervision.

Data availability

The data that support the findings of this study are available from the corresponding author [X. H., Liu], upon reasonable request.

Conflicts of interest

The authors declare that they have no known competing financial interests or personal relationships that could have appeared to influence the work reported in this paper.

Acknowledgements

References

1 É. Hansen, P. M. De Aquim and M. Gutterres, *Ecol. Issues Environ. Impact Assess.*, 2021, **89**, 106597.

2 G. Krishna Priya, M. Javid Mohammed Abu, A. George, M. Aarthy, S. Anbarasan Durai, N. R. Kamini, M. K. Gowthaman, R. Aravindhan, S. Ganesh, R. Chandrasekar and N. Ayyadurai, *J. Cleaner Prod.*, 2016, **126**, 698–706.

3 J. Kanagaraj, T. Senthilvelan, R. C. Panda and S. Kavitha, *J. Cleaner Prod.*, 2015, **89**, 1–17.

4 C. Wei, X. Wang, S. Sun, Q. Lu, X. Zou, L. Xie, P. Huo, D. Hao and X. Liu, *Green Chem.*, 2023, **25**, 5956–5967.

5 X. Liu, W. Wang, X. Wang, S. Sun and C. Wei, *J. Cleaner Prod.*, 2021, **319**, 128658.

6 Md. A. Moktadir, A. Dwivedi and T. Rahman, *J. Cleaner Prod.*, 2022, **348**, 131329.

7 W. Ebabu, M. I. Hossain, M. E. El-Naggar, A. Kechi, S. S. Hailemariam and F. E. Ahmed, *J. Inorg. Organomet. Polym.*, 2022, **32**, 1–14.

8 É. Hansen, J. K. Cardoso, M. Gutterres and P. Monteiro de Aquim, *Process Saf. Environ. Prot.*, 2021, **155**, 466–472.

9 V. Sivakumar, *Process Saf. Environ. Prot.*, 2022, **163**, 703–726.

10 A. B. Mpofu, W. M. Kaira, G. A. Holtman, O. O. Oyekola, R. P. Van Hille and P. J. Welz, *J. Cleaner Prod.*, 2023, **387**, 135872.

11 R. Kumar, A. Basu, B. Bishayee, R. P. Chatterjee, M. Behera, W. L. Ang, P. Pal, M. Shah, S. K. Tripathy, S. Ambika, V. A. Janani, S. Chakrabortty, J. Nayak and B.-H. Jeon, *Environ. Res.*, 2023, **229**, 115881.

12 R. Yu, H. Wang, R. Wang, P. Zhao, Y. Chen, G. Liu and X. Liao, *Water Res.*, 2022, **218**, 118469.

13 R. Li, L. Ren, S. Yu, H. Liu, X. Sun and T. Qiang, *Chem. Eng. J.*, 2024, **482**, 148892.

14 S. Liang, X. Wang, D. Hao, J. Yang and X. Dang, *Process Saf. Environ. Prot.*, 2023, **172**, 753–763.

15 X. Dang, H. Qiu, S. Qu, S. Liang, L. Feng and X. Wang, *ACS Sustainable Chem. Eng.*, 2024, **12**, 3715–3725.

16 Q. Luo, C. Li, W. Zhao, W. Ding, Y. Liu, W. Xiao, H. Liu, X. Pang and J. Sun, *ACS Sustainable Chem. Eng.*, 2024, **12**, 9682–9694.

17 M. Gao, Z. Jiang, W. Ding and B. Shi, *Green Chem.*, 2022, **24**, 375–383.

18 W. Ding, Y. Yi, Y. Wang, J. Zhou and B. Shi, *Carbohydr. Polym.*, 2019, **224**, 115169.

19 D. Hao, X. Wang, X. Liu, R. Su, Z. Duan and X. Dang, *Green Chem.*, 2021, **23**, 9693–9703.

20 C. Wei, X. Wang, W. Wang, S. Sun and X. Liu, *J. Cleaner Prod.*, 2022, **369**, 133229.

21 D. Hao, X. Wang, S. Liang, O. Yue, X. Liu, D. Hao and X. Dang, *Sci. Total Environ.*, 2023, **867**, 161531.

22 W. Huang, Y. Song, Y. Yu, Y. Wang and B. Shi, *J. Leather Sci. Eng.*, 2020, **2**, 8.

23 W. Ding, H. Liu, S. Li, J. Remón, X. Pang and Z. Ding, *ACS Sustainable Chem. Eng.*, 2022, **10**, 17346–17354.

24 W. Ding, J. Remón and Z. Jiang, *Green Chem.*, 2022, **24**, 3750–3758.

25 X. Wang, W. Wang, X. Liu and Y. Wang, *Polym. Adv. Technol.*, 2021, **32**, 1951–1964.

26 D. Hao, X. Wang, X. Liu, X. Zhu, S. Sun, J. Li and O. Yue, *J. Hazard. Mater.*, 2020, **399**, 123048.

27 S. Sun, X. Wang, X. Zhu, X. Liu, P. Guo and Y. Tian, *J. Cleaner Prod.*, 2022, **330**, 129880.

28 H. Jia, Y. Teng, N. Li, D. Li, Y. Dong, D. Zhang, Z. Liu, D. Zhao, X. Guo, W. Di and W. Qin, *ACS Mater. Lett.*, 2022, **4**, 1306–1313.

29 X. Nie, S. Wu, P. Lv, H. Ke, F. Huang and Q. Wei, *Chem. Eng. J.*, 2022, **433**, 134410.

30 C. Qiu, F. Peng, P. Wu, X. Wang, S. Hu, C. Huang, X. Li, D. Xu, H. Li, P.-C. Ma, P. Chen and H. Qi, *Chem. Eng. J.*, 2024, **485**, 149869.

31 S. Wu, J. Fan, W. Wang and D. Yu, *Colloids Surf., A*, 2022, **632**, 127760.

32 Y. Yuan, X. Bao, L. Wu, M. Zhou, Y. Yu, Q. Wang and P. Wang, *Chem. Eng. J.*, 2024, **493**, 152488.

33 R. M. Duke, E. B. Veale, F. M. Pfeffer, P. E. Kruger and T. Gunnlaugsson, *Chem. Soc. Rev.*, 2010, **39**, 3936.

34 L. Jia, S. Zeng, H. Ding, A. T. Smith, A. M. LaChance, M. M. Farooqui, D. Gao, J. Ma and L. Sun, *Adv. Funct. Mater.*, 2021, **31**, 2104427.

35 J. Wan, J. Xu, S. Zhu, J. Li and K. Chen, *Chem. Eng. J.*, 2023, **473**, 145500.

36 L. Yu, X. Qiang, L. Cui, B. Chen, X. Wang and X. Wu, *J. Cleaner Prod.*, 2020, **270**, 122351.

37 X. Liu, Y. Wang, X. Wang and H. Jiang, *Green Chem.*, 2021, **23**, 5924–5935.

38 C. Zou, M. Liang, X. Chen and X. Yan, *J. Appl. Polym. Sci.*, 2014, **131**, 40197.

39 L. Liu, J. Wu, X. Li and Y. Ling, *Sep. Purif. Technol.*, 2013, **10**, 92–100.

40 J. Liu, Y. Sun, C. Wang, K. Hu, C. Jia, G. Wang, Y. Sun, S. Zhang and Y. Zhu, *J. Chromatogr. A*, 2019, **1595**, 91–96.

41 J. Feng, O. O. Oyeneye, W. Z. Xu and P. A. Charpentier, *Ind. Eng. Chem. Res.*, 2018, **57**, 15654–15662.

42 S. Donovan, A. J. Atkinson, N. Fischer, A. E. Taylor, J. Kieffer, J. P. Croue, P. Westerhoff and P. Herckes, *Environ. Sci.: Water Res. Technol.*, 2021, **7**, 1050–1059.

43 B. Kost, W. Gonciarz, A. Krupa, M. Socka, M. Rogala, T. Biela and M. Brzeziński, *Colloids Surf., B*, 2021, **204**, 111801.

44 A. Nechaeva, A. Artyukhov, A. Luss, M. Shtilman, I. Gritskova, A. Shulgin, M. Motyakin, I. Levina, E. Krivoborodov, I. Toropygin, E. Chistyakov, L. Gurevich and Y. Mezhuev, *Polymers*, 2022, **14**, 1727.

45 J. Du, L. Shi and B. Peng, *J. Appl. Polym. Sci.*, 2016, **13**, 43440.

46 C. K. Ozkan, H. Ozgunay and H. Akat, *Int. J. Biol. Macromol.*, 2019, **122**, 610–618.

47 M. J. Chowdhury, Md. T. Uddin, Md. I. Biswas, C. Lyzu, S. Parveen, S. A. Eti and Md. A. Razzaq, *Ind. Crops Prod.*, 2024, **210**, 118159.

48 Y. Wang and L. Hu, *J. Leather Sci. Eng.*, 2022, **4**, 25.

49 H. Wen, Y. Wang, H. Zhu, L. Jin and F. Zhang, *Materials*, 2022, **15**, 1167.

50 N. Yang, J. Ma, J. Shi and Z. Li, *ACS Sustainable Chem. Eng.*, 2023, **11**, 15060–15071.

51 X. He, Y. Huang, H. Xiao, X. Xu, Y. Wang, X. Huang and B. Shi, *Green Chem.*, 2021, **23**, 3581–3587.

52 M. Soni, S. K. Das, P. K. Sahu, U. P. Kar, A. Rahaman and M. Sarkar, *J. Phys. Chem. C*, 2013, **117**, 14338–14347.

53 S. Xu, H. Xiao and B. Shi, *J. Leather Sci. Eng.*, 2022, **4**, 26.

54 K. H. Sizeland, H. C. Wells, S. J. R. Kelly, R. L. Edmonds, N. M. Kirby, A. Hawley, S. T. Mudie, T. M. Ryan and R. G. Haverkamp, *RSC Adv.*, 2017, **7**, 40658–40663.

55 X. Wang, L. Han, S. Qu, L. Feng, S. Liang, C. Wei, X. Liu and X. Dang, *Int. J. Biol. Macromol.*, 2024, **268**, 131682.

56 X. Liu, Y. Wang, X. Wang, T. Han, W. Wang and H. Jiang, *Green Chem.*, 2022, **24**, 2179–2192.

57 V. Suresh, M. Kanthimathi, P. Thanikaivelan, J. R. Rao and B. U. Nair, *J. Cleaner Prod.*, 2001, **9**, 483–491.

58 P. Raji, A. V. Samrot, K. S. Bhavya, M. Sharan, S. Priya and P. Paulraj, *J. Cluster Sci.*, 2019, **30**, 1533–1543.

59 D. Chakraborty, A. H. Quadery and M. A. K. Azad, *Bangladesh J. Sci. Ind. Res.*, 1970, **43**, 553–558.

60 A. D'Aquino, N. Barbani, G. D'Elia, D. Lupinacci, B. Naviglio, M. Seggiani, M. Tomaselli and S. Vitolo, *J. Soc. Leather Technol. Chem.*, 2004, **88**, 47–55.

61 W. R. Wise, S. J. Davis, W. E. Hendriksen, D. J. A. Von Behr, S. Prabakar and Y. Zhang, *Green Chem.*, 2023, **25**, 4260–4270.

62 J. Chen, J. Ma, Q. Fan, W. Zhang and R. Guo, *Chem. Eng. J.*, 2023, **474**, 145453.

63 D. Hao, X. Wang, O. Yue, S. Liang, Z. Bai, J. Yang, X. Liu and X. Dang, *J. Cleaner Prod.*, 2023, **404**, 136917.

64 W. Ding, X. Pang, Z. Ding, D. C. W. Tsang, Z. Jiang and B. Shi, *J. Hazard. Mater.*, 2020, **396**, 122771.

65 W. Ding, J. Zhou, Y. Zeng, Y. Wang and B. Shi, *Carbohydr. Polym.*, 2017, **157**, 1650–1656.

66 Y. Feng, Y. Gu, M. Wang, X. Xu, Y. Liu and D. Li, *Adv. Mater. Interfaces*, 2021, **8**, 2002246.

67 V. Beghetto, L. Agostinis, V. Gatto, R. Samiolo and A. Scrivanti, *J. Cleaner Prod.*, 2019, **220**, 864–872.

68 Y. Shen, J. Ma, Q. Fan, H. Yao, J. Zhang, W. Zhang and H. Yan, *ACS Sustainable Chem. Eng.*, 2023, **11**, 11342–11352.

69 M. Bastanian, A. Olad and M. Ghorbani, *Int. J. Biol. Macromol.*, 2024, **265**, 131133.

70 Y. Yu, Y. Lin, Y. Zeng, Y. Wang, W. Zhang, J. Zhou and B. Shi, *ACS Sustainable Chem. Eng.*, 2021, **9**, 6720–6731.